Anbar Journal Of Engineering Science©
ISSN:1997-9428

Numerical Study Of Turbulent Thermal-Hydraulic Performance Of Al_2o_3-Water Nanofluid In Channel With Triangular Baffles

Mohammed Abed Ahmed [a] *
[a] Department of Mechanical Engineering, College of Engineering, University of Anbar
Ramadi, Anbar, Iraq

ABSTRACT

In this paper, turbulent forced convection of nanofluid flow in channel with isosceles-triangular baffles is numerically investigated over Reynolds number ranges of 5000-10000. One baffle mounted on the bottom wall of channel and another mounted on the top wall. Al_2O_3-water nanofluid with nanoparticles volume fraction of 4% and nanoparticles diameters of 25 nm is used. The governing continuity, momentum and energy equations as well as the low Reynolds number k-ε model of Launder and Sharma have been solved using finite volume method. The effect of baffle height, baffle distance as well as Reynolds number on the flow and thermal characteristics have been presented and discussed. It is found that the enhancement ratio of the average Nusselt number as well as the fraction factor increase with increasing in the baffles height. It is also found that the enhancement ratio of the average Nusselt number increases as the distance of top baffle decrease. Furthermore, the best thermal-hydraulic performance of channel with triangular baffles using nanofluid can be obtained at baffle height of 2.5 mm, distance of the top baffle of 40 mm and Reynolds number of 5000.

Keywords: Thermal-hydraulic Performance, Forced convection, Turbulent flow, Nanofluids, Triangular baffles.

1. INTRODUCTION

In many engineering applications, utilizing compound techniques to improve the thermal performance of heat exchangers is become very important for more compact design of such device. Therefore, suspending naonparticles to the working fluids as well as using turbulators with different shapes lead to significant enhancement in performance of heat exchangers. Forced convection flow and heat transfer characteristics of conventional fluid in channel with different shape of turbulators have been investigated numerically and experimentally by many researchers. Habib et al. [1] experimentally investigated on the turbulent flow and heat transfer characteristics in a rectangular duct with staggered baffles and showed that the heat transfer coefficient and pressure losses increase with increasing the baffle height. Laminar forced convection flow in channel with baffles was numerically investigated by Lopez et al. [2] using a finite volume method. Yang and Hwang [3] studied numerically the turbulent forced convective flow in rectangular channel with porous. The governing continuity, momentum and energy equations as well as the k–

Corresponding Author E mail
drmohaad@gmail.com

ε turbulence model were solved using finite difference method and the results were presented for Reynolds number varying between 10000 and 50000. The results showed the averaged Nusselt number increases with increasing in the height of baffle. Korichi and Oufer [4] numerically investigated on the two-dimensional laminar forced convection flow in a rectangular channel with obstacles mounted on both lower and upper walls and results showed that significant enhancement of the heat transfer. Laminar forced convection heat transfer and fluid flow characteristics in a two-dimensional channel with heated blocks mounted on its bottom wall were numerically studied by Oztop et al. [5]. Results showed that insertion an isothermal bar with triangular cross-section in channel enhanced the heat transfer rate for all values of Reynolds numbers (400-1300). Promvonge et al. [6] investigated numerically the flow and heat transfer characteristics in a square channel with 45^{o} angled baffles over Reynolds number range of 100-1000. The simulations were carried out using finite volume method based on SIMPLE algorithm. Results showed the values of Nusselt number and friction factor increase with the baffle height. Later, Promvonge et al. [7] numerically studied laminar forced convention flow in a square-channel with inline 45° V-shaped baffles mounted on two opposite walls. In this study, SIMPLE algorithm was employed to coupling the velocity and pressure fields. Results showed that the maximum thermal performance factor was about 3.8 at the baffle height ratio of 0.2 and pitch ratio of 1.5 with higher Reynolds number. Turbulent convective heat transfer and flow characteristics in rectangular channel with longitudinal vortex generators was numerically investigated by Min et al. [8]. The governing continuity, momentum and energy equations in addition to k-ε turbulence model were solved using commercial software (Fluent 6.3.26). Results showed that significant enhancement in heat transfer especially with using combined rectangular winglet pair as compared to rectangular winglet pair. Wang and Zhao [9] numerically studied on the performance of a rectangular channel with circular cylinder as vortex generator using Large Eddy Simulation. It was observed that the thermal performance of the channel with circular cylinder was significantly enhanced as a compared with channel without vortex generator. The effect of geometrical parameters on thermal-hydraulic performance of plate-fine heat exchanger with corrugated/vortex-generator plate fin were experimentally conducted by Khoshvaght-Aliabadi et al. [10]. It was found that plate-fine heat exchanger with corrugated/vortex-generator plate fin displays the best thermal-hydraulic performances compared to the corrugated-plate fine heat exchanger or vortex-generator plate fine heat exchanger. The maximum enhancement in heat transfer was about 83.7% for corrugated/vortex-generator plate fin heat exchanger compared to smooth channel.

As for the use of nanofluids to improve the process of heat transfer, there are several numerical and experimental investigations on the flow and heat transfer characteristics of nanofluid in channels at macro and micro-scales. Laminar convective heat transfer of nanofluid in channel with blocks mounted on bottom wall was numerically investigated by Heidary and Kermani [11] using finite volume method. The effect of block number and nanoparticles volume fraction on the local and average Nusselt numbers were presented over Reynolds number range of 10-150. It was found that the highest enhancement in heat transfer about 60% was obtained with using the nanofluid and blocks in channels. Islami et al. [12] numerically studied on the laminar flow and heat transfer of Al_2O_3–water nanofluid in a two dimensional microchannel with and without micromixers. The finite difference method was used to solve the governing equations. In their study, one baffle mounted on the lower wall of microchannel and another

mounted on the upper wall have been employed to enhance the heat transfer in microchannel. The numerical results were presented for different magnitudes of Reynolds numbers, nanoparticle volume fractions as well as the height of baffle. It was found that using baffles and nanoparticle improve the heat transfer rate and increase friction coefficients. Khoshvaght-Aliabadi et al. [13] experimentally and numerically studied on the laminar forced convection of copper-water flow in plate-fin heat exchanger with vortex-generator. In numerical part, the governing equations have been discretized using finite volume approach and solved iteratively using SIMPLEC algorithm. The effect of geometrical parameters as well as nanoparticles volume fraction on thermal performance of heat exchanger have been considered for Reynolds number between 200 and 1800. It was observed that the channel with the wings attach angle of 60^o provide a best thermal performance. Esfe et al. [14] numerically studied laminar mixed convection of Al_2O_3-water nanofluid flow in a horizontal channel with two hot obstacles mounted on the lower wall of channel. The governing equations were discretized using finite volume method and solved iteratively using SIMPLER algorithm. It was found that the maximum enhancement in heat transfer was less than 10% as the nanoparticles volume fraction increases from 0 to 0.05. In addition, the average Nusselt number decrease with increasing in the aspect ratio of obstacle. Abdollahi and Shams [15] studied numerically the effect of the nanoparticles as well as vortex generator on the thermal-hydraulic performance of rectangular channel. It was found that the performance of channel enhanced with the addition nanoparticles to the base fluid and with using vortex generator. Heshmati et al. [16] investigated numerically laminar mixed convection heat transfer of nanofluid flow over a backward facing step with an inclined slotted baffle. The governing equations were discretized using finite volume method and solved iteratively using SIMPLE algorithm over Reynolds number range of 50-400. The effects of geometrical parameters (without baffle, with a solid baffle, with slotted baffle) have been presented and results showed the optimal geometry was the inclined slotted baffle. Laminar and turbulent mixed convection flows of nanofluids over backward facing step in a two-dimensional channel with a rectangular baffle have been numerically investigated by Mohammed et al. [17] using finite volume method based on SIMPLE algorithm scheme. The effect of nanofluid type (Al_2O_3, CuO, SiO_2 and ZnO), nanoparticles volume fractions (0-0.04), nanoparticle diameter (25-80 nm), baffle heights, baffle widths, baffle distance as well as baffle locations on the flow and thermal characteristics were presented and discussed. It was found that SiO_2-water nanofluid gives the highest Nusselt number as a compared to other types of nanofluid. It was also observed that the effect of baffle distance, baffle heights, and baffle locations on heat transfer enhancement were significant, while the effects of baffle width was insignificant.

In present paper, a numerical approach based on the finite volume method is applied to simulate the turbulent flow of alumina–water nanofluid in a channel with triangular baffles. Effects of the baffles height, distance between baffles and the Reynolds number on the thermal-hydraulic performance are investigated and analyzed.

2. MATHEMATICAL MODEL

2.1. Problem Description

The basic geometry of channel considered in the present study is shown in Fig.1. The channel consists of two parallel plates with the distance (H) is 10 mm and length (L) is 400 mm. The channel is composed of three sections; adiabatic section, heated section and adiabatic section. The total length of the heated section is (L_t) 160 mm. The two

adiabatic sections with lengths of 200 mm and 40 mm are located one upstream the heated section and another downstream the heated section, respectively. Two isosceles triangular baffles are mounted at the lower and upper walls of heated section with distance of L_{b1} and L_{b2} from the beginning of the heated section, respectively. Both baffles have uniform dimensions with height (b) of 0.5, 1, 1.5, 2 and 2.5 mm and width (w) of 6 mm. A uniform heat flux conditions with $20\ \mathrm{kW/m^2}$ is applied to the upper and lower walls of heated section. It is assumed that the flow is turbulent, steady, incompressible, and two-dimensional. In addition, the cold mixture of base fluid (water) and the spherical nanoparticles (Al_2O_3) can be assumed as a homogenous mixture.

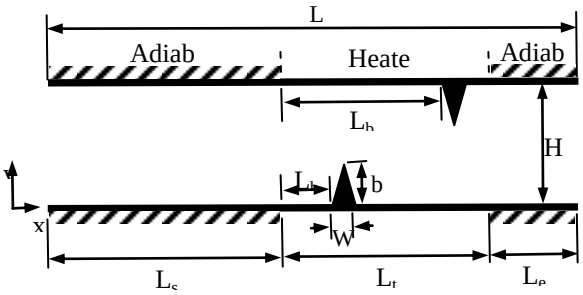

Figure. 1. Physical domain of the present study.

2.2. Governing Equations And Boundary Conditions

The two-dimensional governing equations for turbulent forced convection flow of Al_2O_3-water nanofluid, in Cartesian coordinates are [18]:

Continuity equation:

$$\frac{\partial}{\partial x}(\rho u)+\frac{\partial}{\partial y}(\rho v)=0 \qquad (1)$$

X-Momentum equation:

$$\frac{\partial}{\partial x}(\rho uu)+\frac{\partial}{\partial y}(\rho uv)=-\frac{\partial p}{\partial x}+\frac{\partial}{\partial x}\left[(\mu+\mu_t)\frac{\partial u}{\partial x}\right]+\frac{\partial}{\partial y}\left[(\mu+\mu_t)\frac{\partial u}{\partial y}\right]+\frac{\partial}{\partial x}\left[(\mu+\mu_t)\frac{\partial u}{\partial x}-\frac{2}{3}\rho k\right]+\frac{\partial}{\partial y}\left[(\mu+\mu_t)\frac{\partial v}{\partial x}\right] \qquad (2)$$

Y-momentum equation:

$$\frac{\partial}{\partial x}(\rho uv)+\frac{\partial}{\partial y}(\rho vv)=-\frac{\partial p}{\partial y}+\frac{\partial}{\partial x}\left[(\mu+\mu_t)\frac{\partial v}{\partial x}\right]+\frac{\partial}{\partial y}\left[(\mu+\mu_t)\frac{\partial v}{\partial y}\right]+\frac{\partial}{\partial x}\left[(\mu+\mu_t)\frac{\partial u}{\partial y}\right]+\frac{\partial}{\partial y}\left[(\mu+\mu_t)\frac{\partial v}{\partial y}-\frac{2}{3}\rho k\right] \qquad (3)$$

Energy equation:

$$\frac{\partial}{\partial x}(\rho uT)+\frac{\partial}{\partial y}(\rho vT)=\frac{\partial}{\partial x}\left[\left(\frac{K}{C_p}+\frac{\mu_t}{\mathrm{Pr}_t}\right)\frac{\partial T}{\partial x}\right]+\frac{\partial}{\partial y}\left[\left(\frac{K}{C_p}+\frac{\mu_t}{\mathrm{Pr}_t}\right)\frac{\partial T}{\partial y}\right] \qquad (4)$$

In this paper, Launder-Sharma k-ε model is used to estimate the turbulent dynamic viscosity. These model can be defined as [19]:

Turbulent kinetic energy (k) equation:

$$\frac{\partial}{\partial x}(\rho uk)+\frac{\partial}{\partial y}(\rho vk)=\frac{\partial}{\partial x}\left[\Gamma_k\frac{\partial k}{\partial x}\right]+\frac{\partial}{\partial y}\left[\Gamma_k\frac{\partial k}{\partial y}\right]+P_k-\rho(\varepsilon+\varepsilon_w) \qquad (6)$$

Where ε_w is the dissipation rate at the wall and it can be expressed as:

$$\varepsilon_w=2\frac{\mu}{\rho}\left[\left(\frac{\partial\sqrt{k}}{\partial x}\right)^2+\left(\frac{\partial\sqrt{k}}{\partial y}\right)^2\right] \qquad (7)$$

Turbulent kinetic energy dissipation (ε) equation:

$$\frac{\partial}{\partial x}(\rho u\varepsilon)+\frac{\partial}{\partial y}(\rho v\varepsilon)=\frac{\partial}{\partial x}\left[\Gamma_\varepsilon\frac{\partial\varepsilon}{\partial x}\right]+\frac{\partial}{\partial y}\left[\Gamma_\varepsilon\frac{\partial\varepsilon}{\partial y}\right]+(C_1 f_1 P_k-\rho C_2 f_2\varepsilon)\frac{\varepsilon}{k}+\phi_\varepsilon \qquad (8)$$

Where

$$\phi_\varepsilon=2\mu_t\frac{\mu}{\rho}\left[\left(\frac{\partial^2u}{\partial x^2}\right)^2+\left(\frac{\partial^2v}{\partial x^2}\right)^2+2\left(\frac{\partial^2u}{\partial x\partial y}\right)^2+2\left(\frac{\partial^2v}{\partial x\partial y}\right)^2+\left(\frac{\partial^2u}{\partial y^2}\right)^2+\left(\frac{\partial^2v}{\partial y^2}\right)^2\right] \qquad (9)$$

The production rate of the turbulent kinetic energy (p_k) in Eq. (8) is given as:

$$p_k = \mu_t \left\{ 2\left[\left(\frac{\partial u}{\partial x}\right)^2 + \left(\frac{\partial v}{\partial y}\right)^2 \right] + \left(\frac{\partial u}{\partial y} + \frac{\partial v}{\partial x}\right)^2 \right\} - \frac{2}{3}\rho k \left(\frac{\partial u}{\partial x} + \frac{\partial v}{\partial y}\right) \quad (10)$$

Therefore, the turbulent viscosity can be determined as [19]:

$$\mu_t = C_\mu \, f_\mu \, \rho \, \frac{k^2}{\varepsilon} \quad (11)$$

The empirical constants as well as the turbulent Prandtl number, in above equations, can be expressed as [19]:

$$C_\mu = 0.09,\ C_1 = 1.44,\ C_2 = 1.92,$$
$$\sigma_k = 1.0,\ \sigma_\varepsilon = 1.3,\ \mathrm{Pr}_t = 0.9 \quad \ldots\ldots (12)$$

The wall-damping functions as well as the turbulent Reynolds number are expressed as [20]:

$$f_1 = 1.0 \quad \ldots\ldots\ldots\ldots \quad (13)$$

$$f_2 = 1 - 0.3\exp\left(-\mathrm{Re}_T^2\right) \quad \ldots\ldots \quad (14)$$

$$f_\mu = exp\left[-3.4/\left(1 + 0.02\,Re_T\right)^2\right] \quad \ldots\ldots (15)$$

$$\mathrm{Re}_T = \frac{\rho}{\varepsilon}\frac{k^2}{\mu} \quad \ldots\ldots\ldots\ldots\ldots\ldots\ldots\ldots \quad (16)$$

The corresponding boundary conditions can be expressed as follows [21]:

i. At the inlet section:

$$u = u_{in}, v = 0,\ T = T_{in},\ k = k_{in} = \frac{2}{3}\left(I_o\, u_{in}\right)^2,$$

$$\varepsilon = C\mu^{3/4}\, k_{in}^{3/2} / (0.07 D_h) \quad \ldots\ldots\ldots\ldots \quad (17)$$

ii. At the outlet section:

$$\frac{\partial \mathrm{u}}{\partial \mathrm{x}} = 0,\ \frac{\partial \mathrm{v}}{\partial \mathrm{x}} = 0,\ \frac{\partial \mathrm{T}}{\partial \mathrm{x}} = 0,\ \frac{\partial \mathrm{k}}{\partial \mathrm{x}} = 0,$$

$$\frac{\partial \varepsilon}{\partial \mathrm{x}} = 0 \quad \ldots\ldots\ldots\ldots\ldots\ldots\ldots\ldots\ldots\ldots \quad (18)$$

iii. Along the walls of channel:

$$u = 0,\ v = 0,\ k = 0,\ \varepsilon = 0 \quad \ldots\ldots \quad (19)$$

$$\left.\frac{\partial \mathrm{T}}{\partial \mathrm{y}}\right|_{\mathrm{w}} = -\frac{\mathrm{q_w}}{\mathrm{k_{eff}}}, \text{ along heated walls} \quad \ldots(20)$$

$$\left.\frac{\partial \mathrm{T}}{\partial \mathrm{y}}\right|_{\mathrm{w}} = 0, \text{ along adiabatic walls} \quad \ldots..(21)$$

After solving the governing equations, the flow and thermal field characteristics are obtained which are used to determine the local and the average Nusselt numbers, local skin friction coefficients, friction factor and thermal-hydraulic performance factor. Therefore the local Nussel number can be defined as follows [22]:

$$\mathrm{Nu_x} = \frac{\mathrm{D_h}}{\mathrm{k_{eff}}}\frac{\mathrm{q_w}}{(\mathrm{T_w} - \mathrm{T_b})} \quad \ldots\ldots\ldots\ldots \quad (22)$$

Where T_w is the wall temperature along the channel and T_b is the bulk fluid temperature which can be determined as follows [22]:

$$T_b = \frac{\iint_A \rho u C_p T \, dA}{\iint_A \rho u C_p \, dA} \quad \ldots\ldots\ldots\ldots\ldots \quad (23)$$

The average Nusselt number can be evaluated by integrating the local Nusselt number along the wall of channel as follows:

$$\mathrm{Nu_{av}} = \frac{1}{\mathrm{L_t}} \int_{\mathrm{L_s}}^{\mathrm{L_s}+\mathrm{L_t}} \mathrm{Nu_x}\, \mathrm{dx} \quad \ldots\ldots\ldots\ldots\ldots \quad (24)$$

The local skin-friction coefficient at the wall of channel can be calculated as follows [23]:

$$\mathrm{C_{fx}} = \frac{2}{\rho \mathrm{u_{in}^2}}\left(\frac{\partial \mathrm{u}}{\partial \mathrm{y}}\right)_{\mathrm{w}} \quad \ldots\ldots\ldots\ldots\ldots\ldots \quad (25)$$

The thermal-hydraulic performance factor is defined as [24]:

$$PEC = \frac{(Nu_{av} / Nu_{av,s})}{(f / f_s)^{1/3}} \quad \text{.....(26)}$$

..

Where f is the friction factor which can be expressed as [24]:

$$f = \Delta p \frac{D_h}{L_c} \frac{2}{\rho_{nf} u_{in}^2} \quad \text{.....(27)}$$

The thermophysical properties of AL_2O_3-water nanofluid considered in the current study are the ones used by Zhao et al. [25].

3. NUMERICAL SOLUTION

In the present study, Computational Fluid Dynamics code based on FORTRAN 90 has been developed to perform the numerical solution. The governing equations with appropriate boundary conditions have been discretized using the finite volume method. The SIMPLE algorithm is employed to achieve the coupling between velocity and pressure [26]. The convection terms in the governing equations are discretized using upwind scheme, while the diffusion terms are discretized using second-order central differencing scheme. Furthermore, the Poisson equations are solved to develop the computational mesh. Moreover, all the physical variables have been stored at the same nodes of the computational mesh using collocated grid arrangement [27]. The under-relaxation is applied for all physical variables in order to achieve a better convergence behavior; therefore, the convergence criterion for each variable is set to 10^{-5}.

4. CODE VALIDATION AND GRID INDEPENDENCE TEST

In order to validate the CFD code developed in the this study, the average Nusselt number for the turbulent convective heat transfer of water flow in a straight channel have been calculated and compared with the experimental study of Khoshvaght-Aliabadi et al. [10] and Gnielinski correlation [28] as shown in Fig.2 . In addition, the comparison of the friction factor of present results with the previous experimental result of Khoshvaght-Aliabadi et al. [10] as well as Petukhov correlation [28] is illustrated in Fig.3. According to Figs. (2-3), it can be clearly seen that the results are in a good agreement. For the grid independence test, the local Nusselt number for the lower wall of channel was calculated for different grid size at Re= 5000, b= 2.5 mm, w=6 mm, Lb_1=10 mm and Lb_2=40 mm as shown in Fig.4. It is found that the grid size of 591x91 (591 grid points in x-direction and 91 grid points in y-direction) gives the grid independent solution and it is therefore considered throughout all computations. .

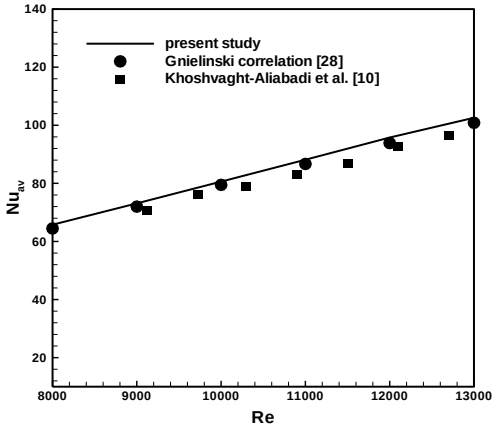

Figure. 2. Comparison of the average Nusselt Number for the present study with previous experimental study of Khoshvaght-Aliabadi et al. [10] as well as Petukhov correlation [28].

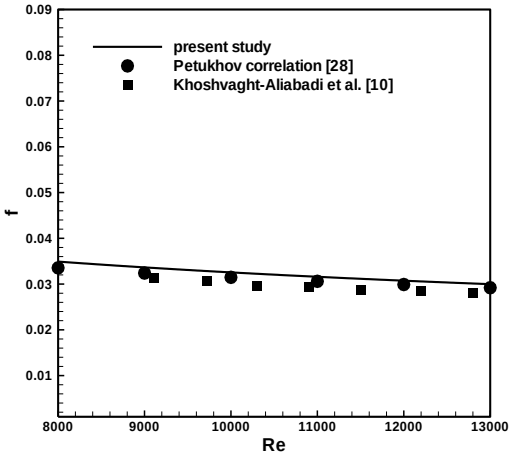

Figure. 3. Comparison of the friction factor for the present study with previous experimental study of Khoshvaght-Aliabadi et al. [10] as well as Petukhov correlation [28].

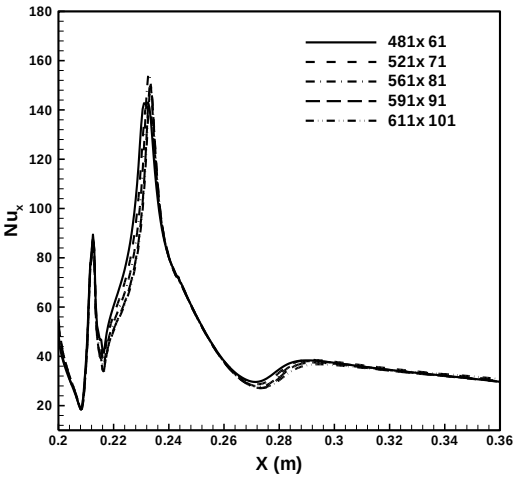

Figure.4. Local Nusselt number for the lower wall of channel for different grid sizes at Re=5000, b=2.5 mm, L_{b1}=10 mm and L_{b2}=40 mm.

5. RESULTS AND DISCUSSION

The effect of baffle height, baffles location as well as Reynolds number on the flow and thermal characteristics in channel with triangular baffles have been presented and discussed in this section. The streamwise velocity and isotherms contours for different baffle height at Re=5000, L_{b1}=10 mm and L_{b2}=40 mm are shown in Fig. 5. It can be seen from velocity contour that the re-circulation zones grow downstream of the top and bottom baffles, as expected. The size of these zones increase with the baffle height. As the baffle height increases, the bottom baffle forces the flow toward the upper wall of channel and creates a small re-circulation zone in front of the top baffle. Looking at isotherms contours, it observed that the presence of the re-circulation zones improve the mixing of cold fluid in core with hot fluid near the walls of channel. Fig. 6 depicts the variation of the local skin friction coefficient along the upper wall of channel for different baffle height at Re=5000, L_{b1}=10 mm and L_{b2}=40 mm. It can be seen from this figure that the friction coefficient in the location of the top baffle (x=0.24 m) increase with the baffle height due to the increase the velocity gradient at this location. Furthermore, the friction coefficient has negative value upstream and downstream the peak value due to presence recirculation regions in front and behind the top baffle especially at baffle height (b) of 2 and 2.5 mm. Fig. 7 shows the local skin-friction coefficient distribution along the upper wall of channel for different locations of the top baffle at Re=5000, L_{b1}=10 mm and b=2.5 mm. It can be observed that the maximum value of friction coefficient occurs in the location of top baffle due to the highest core velocity at this section of channel because the smallest cross section area. The minimum value of friction coefficient occurs downstream the baffle at a point between the separation and reattachment points. Furthermore, when the baffle distance increase (i. e. $L_{b2} \geq 40$ mm), the maximum and minimum values of the friction coefficient become constant this because the bottom baffle does not have any effect on the upper wall of channel.

The effect of baffle height on the local Nusselt number distribution along the upper wall of channel at Re=5000, L_{b1}=10 mm and L_{b2}=40 mm is shown in Fig. 8. It is found that the local Nusselt number in the location of baffle increase with baffle height because the flow accelerate at this location and consequently increase the temperature gradient. Also it is observed that the Nusselt number considerably increase with baffle height at the reattachment point due to presence re-circulation zone behind the baffle which improve the fluid mixing. Fig. 9 gives the variation of local Nusselt number along the upper wall of channel for different location of top baffle at Re=5000, L_{b1}=10 mm and b=2.5 mm. In general, the same trend is found for different location of the top baffle. It is found that the peak value of local Nusselt number decrease as the baffle distance increase and it is shifted downstream the channel. This because of when the distance of top baffle increase, the flow become less disturbed and hence decrease the heat transfer rate.

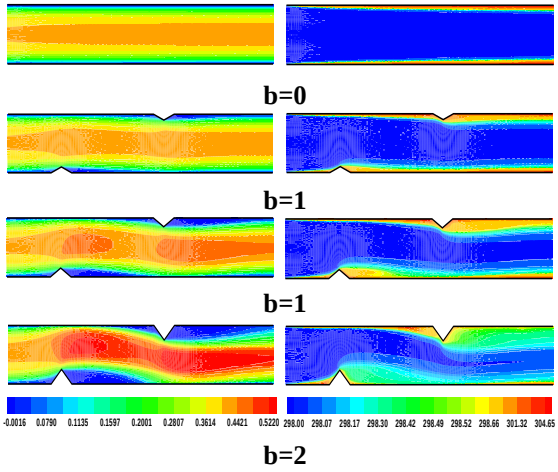

Figure.5. Streamwise velocity (left) and isotherms (right) contours for different baffle heights at Re=5000, L_{b1}=10 mm and L_{b2}=40 mm.

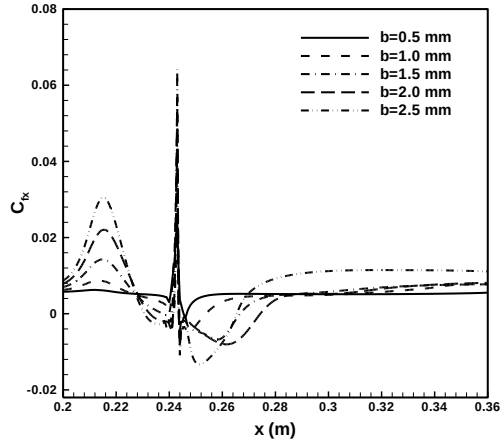

Figure. 6. Variation of local skin friction coefficient along the upper wall of channel for different baffle heights at Re=5000, L_{b1}=10 mm and L_{b2}=40 mm.

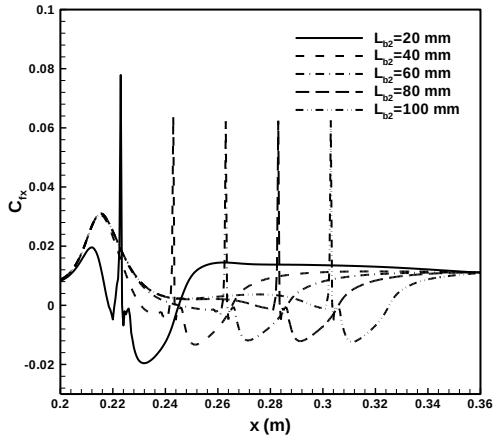

Figure. 7. Variation of local skin friction coefficient along the upper wall of channel for different locations of the top baffle at Re=5000, L_{b1}=10 mm and b=2.5 mm.

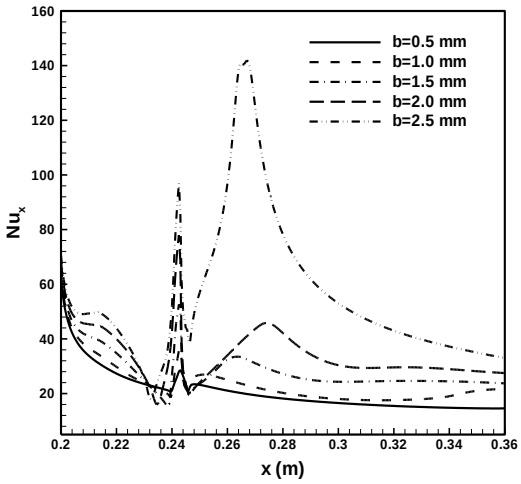

Figure. 8. Variation of local Nusselt number along the upper wall of channel for different baffle heights at Re=5000, L_{b1}=10 mm and L_{b2}=40 mm.

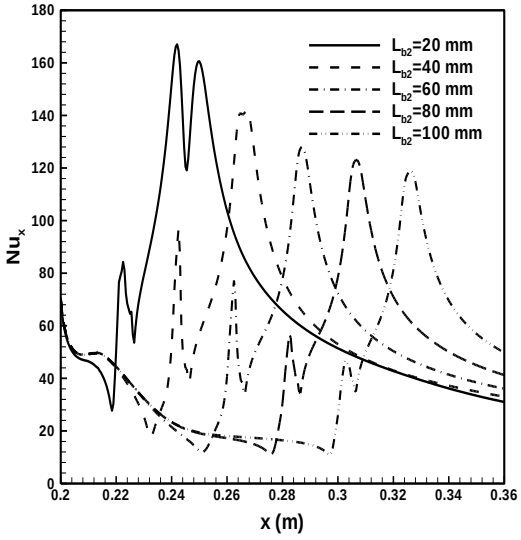

Figure. 9. Variation of local Nusselt number along the upper wall of channel for different locations of the top baffle at Re=5000, L_{b1}=10 mm and b=2.5 mm.

The average friction factor versus Reynolds number for different baffle height at L_{b1}=10 mm and L_{b2}=40 mm is presented in Fig. 10. As expected, it is found that the friction factor increases with baffle height due to increase the size re-circulation zones behind the baffles; as a result, increase the pressure losses. It is also observed that the friction factor increases with increasing the Reynolds number. Fig. 11 displays the effect of baffle distance on the average

friction factor for different Reynolds number at L_{b1}=10 mm and b=2.5 mm. In general, it is observed that the friction factor increase with Reynolds number due to increase the intensity of the reversal flow regions developed in channel. When the distance between the baffles is small (L_{b2}=20 mm), this means that the distance between the recirculation zones of the bottom baffle and the top baffle is small and recirculation zone creates in front of the top baffle. Thus, the flow become more disturbed and consequently increases the friction factor.

The enhancement ratio of the average Nusselt number for Al_2O_3-water nanofluid flow in channel with baffles over the average Nusselt number for pure water in smooth channel (i.e. without baffles) for different baffle height at L_{b1}=10 mm and L_{b2}=40 mm is illustrated in Fig. 12. It can be clearly seen that the average Nusselt number ratio increase with baffle height at a given Reynolds number due to improve the fluid mixing in channel and consequently enhance the heat transfer. It is found that the highest Nusselt number ratio is around 2.73 at Re=5000 and b=2.5 mm. Fig. 13 shows the average Nusselt number for nanofluid flow in channel with baffles over the average Nusselt number for pure water in channel without baffles for different location of the top baffle at L_{b1}=10 mm and b=2.5 mm. It is found that the ratio of Nusselt number increases with the decreasing in the distance of the top baffle. This is because a small recirculation zone creates in front of the top baffle due to the effect of bottom baffle, as mentioned earlier; and hence a further improvement in the fluid mixing. It is observed that he highest Nusselt number ratio is around 2.92 at Re=5000, b=2.5 mm and L_{b2}=20 mm. Figs. (14-15) show the thermal-hydraulic performance factor (PEC) versus Reynolds number for different baffle height and different location of the top baffle, respectively. In general, it is found that the performance factor is greater than unity for all values of the baffle height and the baffle distance considered in this study. This means that the enhancement in the heat transfer is greater than the increasing in friction losses. In addition, it is observed from both figures that the maximum value of performance factor is around 1.622 at b=2.5 mm, L_{b1}=10 mm, L_{b2}=40 mm and Re=5000.

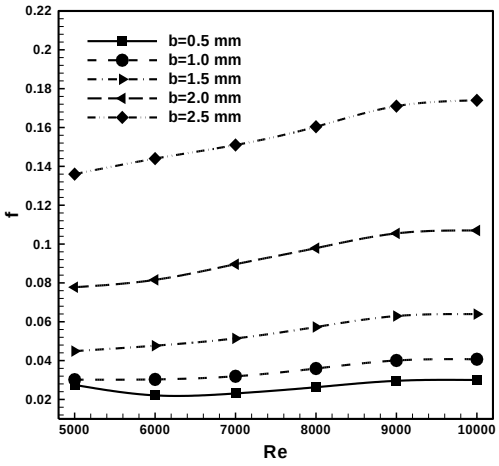

Figure. 10. Friction factor versus Reynolds number for different baffle heights at L_{b1}=10 mm and L_{b2}=40 mm.

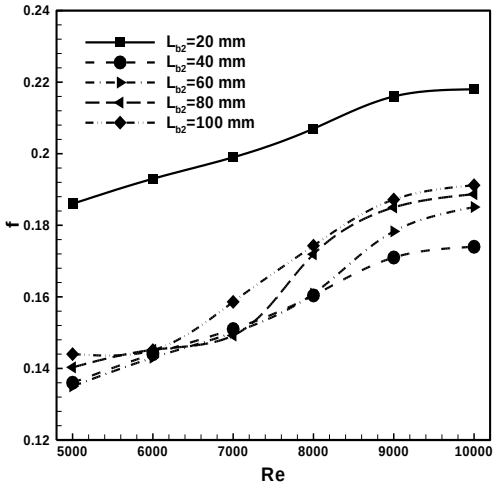

Figure. 11. Friction factor versus Reynolds number for different locations of the top baffle at L_{b1}=10 mm and b=2.5 mm.

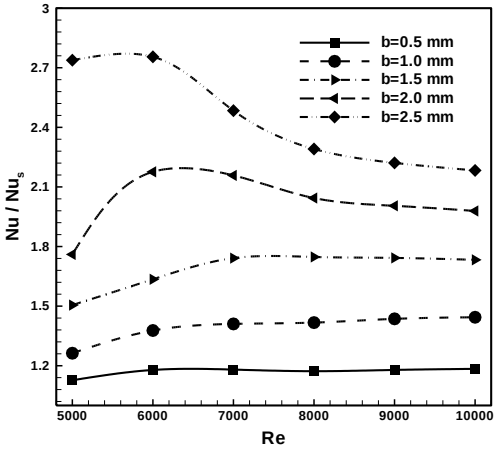

Figure. 12. Average Nusselt number ratio versus Reynolds number for different baffle heights at L_{b1}=10 mm and L_{b2}=40 mm.

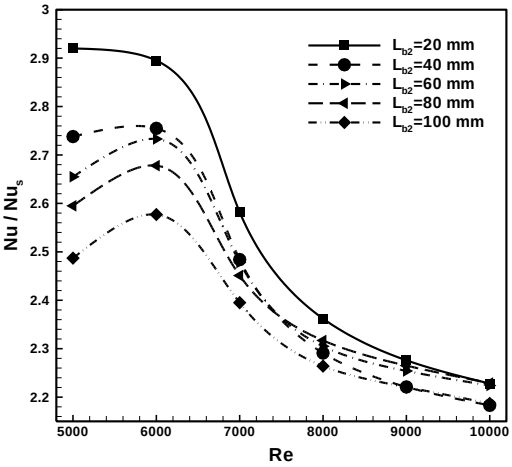

Figure. 13. Average Nusselt number ratio versus Reynolds number for different locations of the top baffle at L_{b1}=10 mm and b=2.5 mm.

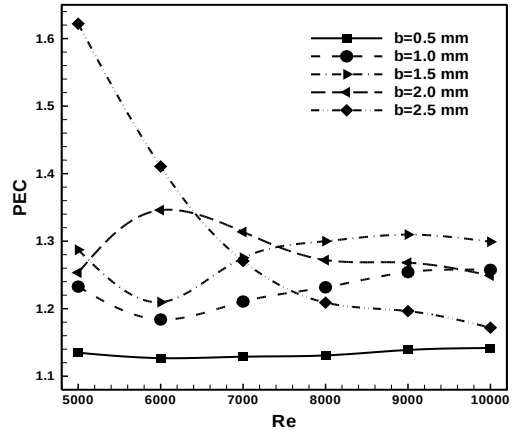

Figure. 14. Thermal-hydraulic performance factor versus Reynolds number for different baffle heights at L_{b1}=10 mm and L_{b2}=40 mm.

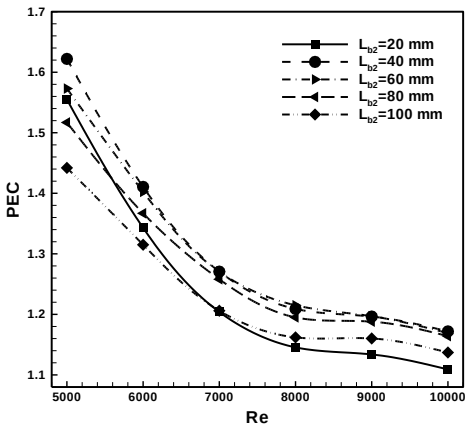

Figure. 15. Thermal-hydraulic performance factor versus Reynolds number for different locations of the top baffle at L_{b1}=10 mm and b=2.5 mm.

6. CONCLUSION

In this paper, the flow and thermal characteristics of turbulent nanofluid flow in channel with triangular baffles have been numerically studied over Reynolds number range of 5000-10000. Al_2O_3-water nanofluid with nanoparticles volume fraction of 4% and nanoparticles diameters of 25 nm have been examined. The governing equations have been discretized using finite volume approach. The effect of flow and geometrical parameters on the flow and thermal field characteristics have been considered. Results show that the enhancement ratio of the Nusselt number and the fraction factor increase with increasing in the baffles height. Also, the enhancement ratio of the average Nusselt number increases as the distance of top baffle decrease. It may conclude that the use Al_2O_3-water nanofluid flow in channel with triangular baffles, at baffle height of 2.5 mm, distance of the top baffle of 40 mm and Reynolds number of 5000, can be achieved the best thermal-hydraulic performance and the corresponding value of the enhancement ratio of average Nusselt number is 2.73

REFERENCES

[1] M.A. Habib, A.M. Mobarak, M.A. Sallak, E.A. Abdel Hadi, R.I. Affify, Experimental investigation of heat transfer and flow over baffles of different heights, ASME J. Heat Transf. 116 (1994) 363–368.

[2] J.R. Lopez, N.K. Anand, L.S. Fletcher, Heat transfer in a three-dimensional channel with baffles, Numer. Heat Transf., Part A: Appl. 30 (1996) 189–205.

[3] Y.T. Yang, C.Z. Hwang, Calculation of turbulent flow and heat transfer in a porous baffled channel, Int. J. Heat Mass Transf. 46 (2003) 771–780.

[4] A. Korichi, L. Oufer, Heat transfer enhancement in oscillatory flow in channel with periodically upper and lower walls mounted obstacles, Int. J. Heat Fluid Flow 28 (5) (2007) 1003–1012.

[5] H.F. Oztop, Y. Varol, D.E. Alnak, Control of heat transfer and fluid flow using a triangular bar in heated blocks located in a channel, Int. Commun. Heat and Mass Transfer 36 (2009) 878-885.

[6] P. Promvonge, S. Sripattanapipat, S. Kwankaomeng, Laminar periodic flow and heat transfer in square channel with 45^{o} inline baffles on two opposite walls, Int. J. Therm. Sci. 49 (2010) 963–975.

[7] P. Promvonge, W. Jedsadaratanachai, S. Kwankaomeng, C. Thianpong, 3D simulation of laminar flow and heat transfer in V-baffled square channel, Int. Commun. Heat and Mass Transfer, 39 (2012) 85-93.

[8] C. Min, C. Qi, E. Wang, L. Tian, Y. Qin, Numerical investigation of turbulent flow and heat transfer in a channel with novel longitudinal vortex generators, Int. J. Heat and Mass Transfer, 55(2012), 7268-7277.

[9] J. Wang, Y. Zhao, Heat and fluid flow characteristics of a rectangular channel with a small diameter circular cylinder as vortex generator, International Journal of Thermal Sciences, 92 (2015) 1-13.

[10] M. Khoshvaght-Aliabadi, M. Khoshvaght, P. Rahnama, Thermal-hydraulic characteristics of plate-fin heat exchangers with corrugated/vortex-generator plate-fin (CVGPF), Applied Thermal Engineering 98 (2016) 690-701.

[11] H. Heidary, M. J. Kermani, Heat transfer enhancement in a channel with block (s) effect and utilizing Nano-fluid, Int. J. Thermal Sciences 57 (2012) 163-171.S.B.

[12] Islami, B. Dastvareh, R. Gharraei, Numerical study of hydrodynamic and heat transfer of nanofluid flow in microchannels containing micromixer, International Communications in Heat and Mass Transfer 43 (2013) 146-154.

[13] M. Khoshvaght-Aliabadi, F. Hormozi, A. Zamzamian, Effects of geometrical parameters on performance of plate-fin heat exchanger: Vortex-generator as core surface and nanofluid as working media, Applied Thermal Engineering 70 (2014) 565-579.

[14] M. H. Esfe, A. A. A. Arani, A. H. N., W. M. Yan, A. Karimipour, Mixed convection heat transfer from surface-mounted block heat sources in a horizontal channel with nanofluids, Int. J. Heat and Mass Transfer 89 (2015) 783-791.

[15] A. Abdollahi, M. Shams, Optimization of heat transfer enhancement of nanofluid in a channel with winglet vortex generator, Applied Thermal Engineering 91 (2015) 1116-1126.

[16] A. Heshmati, H. A. Mohammed, A. N. Darus, Mixed convection heat transfer of nanofluids over backward facing step having a slotted baffle, Applied Mathematics and Computation 240 (2014) 368-386.

[17] H.A. Mohammed, O. A. Alawi, M.A.Wahid, Mixed convective nanofluid flow in a channel having backward-facing step with a baffle, Powder Technology 275 (2015) 329–343.

[18] L. C. Yang, Y. Asako, Y. Yamaguchi, M. Faghri, Numerical prediction of transitional characteristics of flow and heat transfer in a corrugated duct, Journal of heat transfer, 119 (1997), 62-69.

[19] J. Blazek, Computational Fluid Dynamics: Principles and Applications: Principles and Applications, 2nd edition. Elsevier, 2005.

[20] C. J. Chen, S.Y. Jaw, Fundamentals of turbulence modelling, Taylor and Francis, 1997.

[21] L. Zhang, D. Che, Influence of corrugation profile on the thermal hydraulic performance of cross-corrugated plates, Numerical Heat Transfer, Part A, 59 (2011) 267-296.

[22] M. Kalteh, A. Abbassi, M. Saffar-Avval, J. Harting, Eulerian–Eulerian two-phase numerical simulation of nanofluid laminar forced convection in a microchannel, Int. J. Heat and Fluid Flow, 32(2011), 107-116.

[23] H. S. Choi, K. Suzuki, Large eddy simulation of turbulent flow and heat transfer in a channel with one wavy wall. Int. J. heat and fluid flow, 26(2005), 681-694.

[24] O. Manca, S. Nardini, D. Ricci, A numerical study of nanofluid forced convection in ribbed channels, Applied Thermal Engineering 37(2012) 280-292.

[25] N. Zhao, J. Yang, S. Li, Q. Wang, Numerical investigation of laminar thermal-hydraulic performance of Al_2O_3-water nanofluids in offset strip fins channel. Int. Commun. Heat and Mass Transfer 75 (2016) 42-51.

[26] H.K. Versteeg, W. Malalasekera, An introduction to computational fluid dynamics the finite volume method, 2nd edition. Longman Scientific and Technical, England, 2007.

[27] C. M. Rhie, W. L. Chow, Numerical study of the turbulent flow past an airfoil with trailing edge separation, AIAA journal, 21(1983), 1525-1532.

[28] F. P. Incropera, D. P. DeWitt, L.B. Theodore, S. L. Adrienne, Fundamentals of Heat and Mass Transfer, 6th edition, John Wiley & Sons, Hoboken, 2007.

NOMENCLATURE

b	baffle height, mm
C_1, C_2, C_μ	empirical constant for turbulence model
C_f	skin-friction coefficient
C_p	specific heat, J/Kg k
D_h	hydraulic diameter, mm
h	heat transfer coefficients, ($W/m^2.^oC$)
H	height of channel, mm
L_s, L_e	lengths of unheated sections, mm
L_t	length of heated section, mm
f	friction factor
f_1, f_2, f_μ	damping function
k	turbulent kinetic energy, m/s^2
k	thermal conductivity, W/m. ^oC
Nu	Nusselt number

p	pressure, pa
PEC	thermal-hydraulic performance factor
q_w	heat flux, kW/m^2
Pr_t	Turbulent Prandtl number
Re	Reynolds number
T	temperature, ^{o}C
u ,v	velocities components, m/s
x, y	2D Cartesian coordinates, mm

Greek Symbols

$\sigma_k, \sigma_\varepsilon$	empirical constant for turbulence model
ε	dissipation rate of turbulent kinetic energy, m^2/s^3
μ	dynamic viscosity, Ns/m^2
μ_t	turbulent dynamic viscosity, N s/m^2
ρ	density, kg/m^3
Δp	pressure drop, pa
Γ	Diffusion coefficient

Subscripts

av	average value
b	bulk fluid
eff	effective
f	base fluid
in	inlet
nf	nanofluid
p	particles
s	smooth channel
o	outlet
w	wall
x	local value